Available online at www.sciencedirect.com
ScienceDirect
International Journal of Thermal Sciences 46 (2007) 768–778
International Journal of Thermal Sciences
www.elsevier.com/locate/ijts

Numerical study of local heat transfer coefficient and fin efficiency of wavy fin-and-tube heat exchangers ☆

Y.B. Tao, Y.L. He *, J. Huang, Z.G. Wu, W.Q. Tao

State Key Laboratory of Multiphase Flow in Power Engineering, School of Energy & Power Engineering, Xi'an Jiaotong University, Xi'an, Shaan xi 710049, China

Received 13 April 2006; received in revised form 7 October 2006; accepted 7 October 2006

Available online 17 November 2006

Abstract

Three-dimensional numerical simulations were performed for laminar flow of wavy fin-and-tube heat exchangers by using body-fitted coordinates (BFC) method with fin efficiency effect accounted. The prediction results of average Nusselt number, friction factor and fin efficiency were compared with the related experimental correlations [R.C. Xin, H.Z. Li, H.J. Kang, W. Li, W.Q. Tao, An experimental investigation on heat transfer and pressure drop characteristics of triangular wavy fin-and-tube heat exchanger surfaces, J. Xi'an Jiaotong Univ. 28 (2) (1994) 77–83] and Schmidt approximation [T.E. Schmidt, Heat transfer calculations for extended surfaces, Refrigerating Engineering (April 1949) 351–357]. For Reynolds numbers based on the tube outside diameter ranging from 500 to 4000, the mean deviation is 3.3% for Nusselt number, 1.9% for friction factor and 3.6% for fin efficiency. The distributions of local Nusselt number and fin efficiency on fin surface were studied at wavy angle equal to 0° (plain plate fin), 10° and 20° respectively. The local Nusselt number decreases along the air flow direction, but fin efficiency increases in general. The wavy angle can greatly affect the distributions of local Nusselt number and fin efficiency, and make the distributions present fluctuation along the flow direction. The result also shows that the fin efficiency at the inlet region of wavy fin is larger than that of plain plate fin at the same region. With the increase of Reynolds number, the effects of wavy angle on the distributions of local Nusselt number and fin efficiency are more and more significant.

Keywords: Wavy fin-and-tube heat exchanger; Numerical simulation; Local Nusselt number; Local fin efficiency

1. Introduction

Fin-and-tube heat exchangers are employed in varieties of engineering applications, for example, applications in such areas like air conditioning units, process gas heaters and coolers, compressor intercoolers, etc. Since majority of the thermal resistance of fin-and-tube heat exchangers is on the air side, improving air side fin configuration and enhancing its heat transfer is the most effective way to improve the performance of the heat exchangers. The conventional method for enhancing air side heat transfer is by adopting the wavy and slot fins. A lot of experimental and/or numerical studies have been conducted on airside heat transfer performance of wavy fin-and-tube heat exchangers. Wang et al. [1,2] made extensive experiments on the heat transfer and pressure drop characteristics of wavy fin and tube heat exchangers. Wongwises and Chokeman [3] experimentally investigated the effects of fin pitch and number of tube rows on the air side performance of herringbone wavy fin and tube heat exchangers. Jang and Chen [4] numerically studied the heat transfer and fluid flow in a three-dimensional wavy fin-and-tube heat exchanger. Manglik et al. [5] analyzed the effects of fin density on low Reynolds number forced convection in three-dimensional wavy-plate-fin compact channels by numerical simulation.

The foregoing literature review shows that in all the previous studies, the main emphasis was placed on studying the effects of parameters on the average air side heat transfer and pressure drop characteristics of wavy fin-and-tube heat exchanger, little discussions about fin efficiency have been reported. Many

☆ The present work is supported by the National Science Fund for Distinguished Young Scholars from the National Natural Science Foundation of China (No. 50425620), and the Key Grant Project of Chinese Ministry of Education (No. 306014).

* Corresponding author. Tel.: +86 29 82663851; fax: +86 29 82669106.
E-mail address: yalinghe@mail.xjtu.edu.cn (Y.L. He).

1290-0729/$ – see front matter
doi:10.1016/j.ijthermalsci.2006.10.004

Nomenclature

A	total surface or cross-sectional area	m^2
A_f	fin surface area	m^2
A_o	total surface area	m^2
C_p	specific heat	$J\,kg^{-1}\,K^{-1}$
D	tube outside diameter	m
f	friction factor	
F_p	fin pitch	m
h	heat transfer coefficient	$W\,m^{-2}\,K^{-1}$
k	thermal conductivity	$W\,m^{-1}K^{-1}$
L	fin length along flow direction	m
N	the number of control volume or point	
n	tube row numbers	
Nu	total Nusselt number $(h \cdot D)/k$	
$Nu_{i,j}$	local Nusselt number	
p	pressure	Pa
Δp	pressure drop in flow direction	Pa
P_l	longitudinal tube pitch	m
P_t	transverse tube pitch	m
Q	heat transfer capacity	W
q_w	heat flux at fin surface	$W\,m^{-2}$
r	tube outside radius	m
Re	Reynolds number based on tube outer side diameter $(U_c D/\upsilon)$	
S	tube row pitch	m
T	temperature	K
$\overline{T}$	bulk average temperature	K
$\overline{p}$	bulk average pressure	Pa
u, v, w	x, y, z velocity components	$m\,s^{-1}$
U_c	velocity at the minimum cross sectional area	m^{-1}
U, V, W	transformed velocity	$m\,s^{-1}$
x, y, z	Cartesian coordinates	
X_L	$\sqrt{(P_t/2)^2 + P_l^2/2}$, geometric parameter	m
X_M	$P_t/2$, geometric parameter	m

Greek symbols

α	wavy angle	°
μ	dynamic viscosity	Pa s
υ	kinematic viscosity	$m^2\,s^{-1}$
ρ	density	$kg\,m^{-3}$
λ	thermal conductivity	$W\,m^{-1}\,K^{-1}$
ξ, η, ζ	body-fitted coordinates	
η	fin efficiency	
Γ	boundary segment	

Subscripts

cal	calculation results
exp	experiment results
in	inlet parameters
m	mean or average value
o	air side
out	outlet parameters
w	at fin surface conditions
wt	at tube surface conditions
i, j	local values

investigators [6–8] also applied the uniform heat transfer coefficient assumption for fin efficiency calculation. However, it is well known that there exists a very complex flow pattern within a wavy fin-and-tube heat exchanger due to its three-dimensional nature and flow separations, which causes local variations of the heat transfer coefficient. Jones and Russell [9], Saboya and Sparrow [10], Rosman et al. [11] and Ay et al. [12] demonstrate that there exists a great variation of the heat transfer rate on the fin surface of the plate fin-and-tube heat exchanger. This also implies that the heat transfer coefficient on the fin surface is very nonuniform and the actual steady-state heat transfer coefficient on the fin surface should be the function of position. But it is very difficult to measure the local heat transfer coefficient on the fins, because for this purpose the local fin temperature and local heat flux are needed. The study of the distributions of the local heat transfer coefficient and fin efficiency on the fin surface is an important task to design high-performance heat exchangers because the results can be used to point out the areas where the enhancement is mostly needed and effective.

In this study, a 3D numerical simulation of the air side heat transfer and flow characteristics of wavy fin-and-tube heat exchangers was performed by body-fitted coordinates system with taking fin efficiency into account. The predictions of average Nusselt number, friction factor and fin efficiency were compared with the available experimental correlations and Schmidt approximation [13]. The local Nusselt number and fin efficiency distributions were investigated. The variations of local Nusselt number and fin efficiency along the air flow direction and the distributions of local Nusselt number and fin efficiency on the whole fin surface were obtained. The effects of wavy angle and Reynolds number on temperature, local Nusselt number and fin efficiency distributions were studied at wavy angle equal to 0° (plain plate fin), 10° and 20°.

2. Model description

2.1. Physical model

The schematic diagram of the wavy fin-and-tube heat exchanger is shown in Fig. 1 with two rows of tubes in the flow direction. Table 1 lists all the geometric dimensions for this heat exchanger. The air flow direction is x-direction, fin span wise direction is y-direction and fin thickness direction is z-direction, as shown in Figs. 1 and 2. Fig. 2 shows the computational domain of the wavy fin. The actual length of the computation domain was 7.5 times of the original heat transfer zone. The domain was extended 1.5 times of the original heat transfer zone for the entrance section to ensure the inlet uniformity, and at the exit, the domain was extended 5 times of the original heat transfer zone in order to make sure that the exit flow boundary has no flow recirculation and the local one-

Table 1
Geometric dimension for the studied heat exchanger

Tube row number	2
Tube outside diameter (mm)	10.55
Transverse pitch (mm)	25.0
Longitudinal pitch (mm)	21.65
Fin pitch (mm)	2.0
Fin thickness (mm)	0.2
Wavy angle (°)	17.44
Wavy length (mm)	10.825
Air flow direction length (mm)	43.3

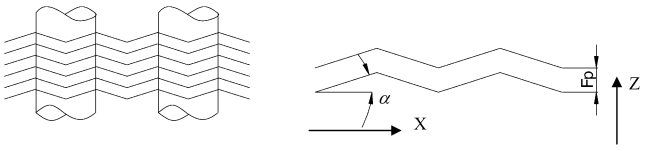

Fig. 1. Schematic diagram of a wavy fin-and-tube heat exchanger.

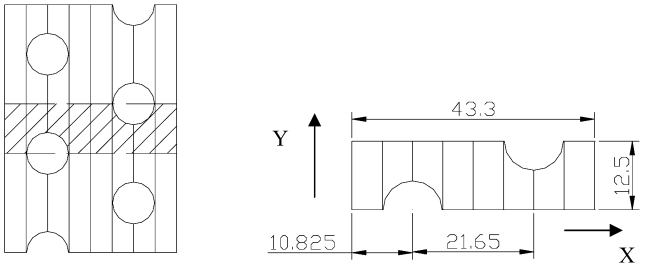

Fig. 2. Computational domain of the fin.

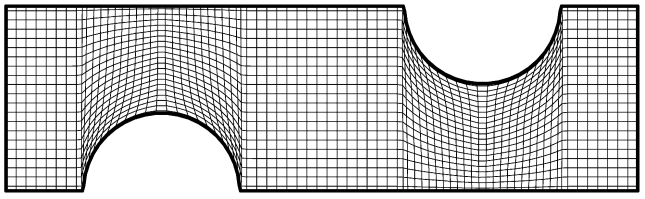

Fig. 3. Schematic of grid systems generated by body-fitted coordinates.

way method can be used for the numerical treatment of the exit flow boundary condition. The grid system for the computation domain generated by BFC is shown in Fig. 3, where the upstream and downstream parts of the computation domain are not presented in order to save the space. In these two extended computation domains a much coarser grid was adopted to save the computing resource.

2.2. Grids generation technique

The traditional method to simulate the fin-and-tube heat exchanger was mostly performed in Cartesian coordinates by adopting the step-approaching method at the tube surface. But this approximation method will cause some errors related to the grid precision, the coarser of the grid, the larger of the error. Too fine grid will lead to more computation time, and the complicated computation domain makes the use of step-approaching method more difficult. In this paper, the body-fitted coordinates were adopted, which helps to transform the complex computational domain in physical space into a simple domain in the computational space.

The basic idea of the body-fitted coordinate is to numerically generate a curvilinear coordinate system having coordinate lines coincident with each boundary of the real computational domain, regardless of the shapes of these boundaries. This is implemented by solving elliptic partial differential equations. Constant values of one of the curvilinear coordinates are specified as Dirichlet boundary condition on each boundary. Values of the other coordinates are either specified by a monotonic variation over a boundary as Dirichlet boundary conditions, or determined by Neumann boundary conditions. In the latter case, the curvilinear coordinate lines can be made to intersect the boundary according to some specified conditions, such as being normal or parallel to some given directions. It is also possible to exercise control over the spacing of the curvilinear coordinate lines in the field in order to concentrate lines in regions of expected higher gradients. In any case, the numerical generation of the coordinate system is done automatically for any shape boundaries, requiring only the input of points on the boundary.

In order to obtain a grid in the computational space, a grid system generating method needs to be developed. The simplest equation that could be used to generate the grid is Laplace equation,

$$\nabla^2 \xi_i = 0, \quad i = 1, 2, 3 \tag{1}$$

The commonly used grid generation techniques are based on the Poisson equation proposed in Thompson et al. [14]. The 3D Poisson equation in physical space can be expressed as:

$$\begin{aligned}
&\frac{\partial^2 \xi}{\partial^2 x} + \frac{\partial^2 \xi}{\partial^2 y} + \frac{\partial^2 \xi}{\partial^2 z} = P(\xi, \eta, \varsigma) \\
&\frac{\partial^2 \eta}{\partial^2 x} + \frac{\partial^2 \eta}{\partial^2 y} + \frac{\partial^2 \eta}{\partial^2 z} = Q(\xi, \eta, \varsigma) \\
&\frac{\partial^2 \varsigma}{\partial^2 x} + \frac{\partial^2 \varsigma}{\partial^2 y} + \frac{\partial^2 \varsigma}{\partial^2 z} = R(\xi, \eta, \varsigma)
\end{aligned} \tag{2}$$

where P, Q and R are functions for controlling the spacing between coordinate lines. The above partial differential equations are subject to a set of Dirichlet boundary conditions, such as:

$$\begin{bmatrix} \xi \\ \eta \\ \zeta \end{bmatrix} = \begin{bmatrix} \xi_1(x, y, z) \\ \eta_1 \\ \zeta_1(x, y, z) \end{bmatrix}, \quad (x, y, z) \in \Gamma \tag{3}$$

where η_1 is a specified constant, $\xi_1(x, y, z)$ and $\zeta_1(x, y, z)$ are specified monotonic functions on a boundary segment Γ.

The above equations are transformed into the computational space where the Cartesian coordinates are the dependent variables. Then we have

$$\begin{aligned}
&\alpha_{11} x_{\xi\xi} + \alpha_{22} x_{\eta\eta} + \alpha_{33} x_{\zeta\zeta} + 2\alpha_{12} x_{\xi\eta} + 2\alpha_{13} x_{\xi\zeta} + 2\alpha_{23} x_{\eta\zeta} \\
&\quad + J^2 (P x_\xi + Q x_\eta + R x_\zeta) = 0 \\
&\alpha_{11} y_{\xi\xi} + \alpha_{22} y_{\eta\eta} + \alpha_{33} y_{\zeta\zeta} + 2\alpha_{12} y_{\xi\eta} + 2\alpha_{13} y_{\xi\zeta} + 2\alpha_{23} y_{\eta\zeta} \\
&\quad + J^2 (P y_\xi + Q y_\eta + R y_\zeta) = 0 \\
&\alpha_{11} z_{\xi\xi} + \alpha_{22} z_{\eta\eta} + \alpha_{33} z_{\zeta\zeta} + 2\alpha_{12} z_{\xi\eta} + 2\alpha_{13} z_{\xi\zeta} + 2\alpha_{23} z_{\eta\zeta} \\
&\quad + J^2 (P z_\xi + Q z_\eta + R z_\zeta) = 0
\end{aligned} \tag{4}$$

where $\alpha_{jk} = \sum_{m=1}^{3} \beta_{mj}\beta_{mk}$, and β_{mk} is the cofactor of the (m,k) element in the matrix M:

$$M = \begin{bmatrix} x_\xi & x_\eta & x_\zeta \\ y_\xi & y_\eta & y_\zeta \\ z_\xi & z_\eta & z_\zeta \end{bmatrix}, \quad \text{and} \quad J = \det|M| \tag{5}$$

Thus,

$$\begin{aligned}
\alpha_{11} &= \beta_{11}^2 + \beta_{21}^2 + \beta_{31}^2 \\
\alpha_{22} &= \beta_{12}^2 + \beta_{22}^2 + \beta_{32}^2 \\
\alpha_{33} &= \beta_{13}^2 + \beta_{23}^2 + \beta_{33}^2 \\
\alpha_{12} &= \beta_{11}\beta_{12} + \beta_{21}\beta_{22} + \beta_{31}\beta_{32} \\
\alpha_{13} &= \beta_{11}\beta_{13} + \beta_{21}\beta_{23} + \beta_{31}\beta_{33} \\
\alpha_{23} &= \beta_{12}\beta_{13} + \beta_{22}\beta_{23} + \beta_{32}\beta_{33}
\end{aligned} \tag{6}$$

The transformed boundary conditions are:

$$\begin{bmatrix} x \\ y \\ z \end{bmatrix} = \begin{bmatrix} f_1(\xi,\eta_1,\zeta) \\ f_2(\xi,\eta_1,\zeta) \\ f_3(\xi,\eta_1,\zeta) \end{bmatrix}, \quad (\xi,\eta_1,\zeta) \in \Gamma^* \tag{7}$$

where $f_1(\xi,\eta_1,\zeta)$, $f_2(\xi,\eta_1,\zeta)$ and $f_3(\xi,\eta_1,\zeta)$ are determined by the known shape of the boundary segment Γ and the specified distribution of ξ and ζ thereon. Γ^* is the boundary segment of Γ in the transformed space.

In order to improve the quality of the generated grid system, especially for the parts of wave crest and wave trough, in this paper the final grid systems were generated by the block structured method with body-fitted coordinates [15]. The grid systems generated by body-fitted coordinates for the fin part are shown in Fig. 3.

2.3. The governing equations

The governing equations for the forced steady, laminar, incompressible fluid flow and heat transfer in the physical space are:

Continuity equation:

$$\frac{\partial}{\partial x_i}(\rho u_i) = 0 \tag{8}$$

Momentum equation:

$$\frac{\partial}{\partial x_i}(\rho u_i u_k) = \frac{\partial}{\partial x_i}\left(\mu \frac{\partial u_k}{\partial x_i}\right) - \frac{\partial p}{\partial x_k} \tag{9}$$

Energy equation:

$$\frac{\partial}{\partial x_i}(\rho u_i T) = \frac{\partial}{\partial x_i}\left(\frac{k}{C_p}\frac{\partial T}{\partial x_i}\right) \tag{10}$$

The governing equations in the computational space are:

$$\frac{\partial}{\partial \xi}(\rho U) + \frac{\partial}{\partial \eta}(\rho V) + \frac{\partial}{\partial \varsigma}(\rho W) = 0 \tag{11}$$

$$\begin{aligned}
&\frac{\partial}{\partial \xi}(\rho U\Phi) + \frac{\partial}{\partial \eta}(\rho V\Phi) + \frac{\partial}{\partial \varsigma}(\rho W\Phi) \\
&\quad = \frac{\partial}{\partial \xi}\left(\frac{\alpha}{J}\Gamma^{\Phi}\frac{\partial \Phi}{\partial \xi}\right) + \frac{\partial}{\partial \eta}\left(\frac{\beta}{J}\Gamma^{\Phi}\frac{\partial \Phi}{\partial \eta}\right) \\
&\qquad + \frac{\partial}{\partial \varsigma}\left(\frac{\gamma}{J}\Gamma^{\Phi}\frac{\partial \Phi}{\partial \varsigma}\right) + JS
\end{aligned} \tag{12}$$

where U, V and W are velocity components in transformed space and Φ is the general variable.

$$\begin{aligned}
U &= \alpha_1 u + \alpha_2 v + \alpha_3 w \\
V &= \beta_1 u + \beta_2 v + \beta_3 w \\
W &= \gamma_1 u + \gamma_2 v + \gamma_3 w \\
J &= x_\xi y_\eta z_\zeta + x_\eta y_\zeta z_\xi + x_\zeta y_\xi z_\eta \\
&\quad - x_\zeta y_\eta z_\xi - x_\eta y_\xi z_\zeta - x_\xi y_\zeta z_\eta
\end{aligned} \tag{13}$$

2.4. Boundary conditions

The fluid is assumed to be incompressible with constant property and the flow is laminar and in steady state condition. In order to study the fin efficiency distribution, the heat conductivity of the fin must be considered. In the paper, the fin surfaces are considered as a part of the solution domain and will be treated as a special type of fluid. The temperature of the tube surface is higher than that of the inlet air. The boundary conditions are described for the three regions as follows.

(a) In the upstream extended region (domain inlet)
At the inlet boundary:

$$\begin{aligned}
&u = u_{\text{in}} = \text{const}, \qquad v = w = 0 \\
&T = T_{\text{in}} = \text{const}
\end{aligned} \tag{14a}$$

At the upper and lower boundaries:

$$\frac{\partial u}{\partial z} = \frac{\partial v}{\partial z} = 0, \qquad w = 0, \qquad \frac{\partial T}{\partial z} = 0 \tag{14b}$$

At the front and back boundaries:

$$\frac{\partial u}{\partial y} = \frac{\partial w}{\partial y} = 0, \qquad v = 0, \qquad \frac{\partial T}{\partial y} = 0 \tag{14c}$$

(b) In the downstream extended region (domain outlet)
At the upper and lower boundaries:

$$\frac{\partial u}{\partial z} = \frac{\partial v}{\partial z} = 0, \qquad w = 0, \qquad \frac{\partial T}{\partial z} = 0 \tag{15a}$$

At the front and back boundaries:

$$\frac{\partial u}{\partial y} = \frac{\partial w}{\partial y} = 0, \qquad v = 0, \qquad \frac{\partial T}{\partial y} = 0 \tag{15b}$$

At the outlet boundary:

$$\frac{\partial u}{\partial x} = \frac{\partial v}{\partial x} = \frac{\partial w}{\partial x} = \frac{\partial T}{\partial x} = 0 \tag{15c}$$

(c) In the fin coil region
At the upper and lower boundaries:
Velocity condition:

$$u = v = w = 0 \tag{16a}$$

Temperature condition: periodic conditions
At the front and back boundaries:
Fluid region:

$$\frac{\partial u}{\partial y} = \frac{\partial w}{\partial y} = 0, \qquad v = 0, \qquad \frac{\partial T}{\partial y} = 0 \tag{16b}$$

Fin surface region:

$$u = v = w = 0, \qquad \frac{\partial T}{\partial y} = 0 \tag{16c}$$

Tube region:

$$u = v = w = 0, \qquad T = T_{\mathrm{wt}} = \mathrm{const} \tag{16d}$$

3. Numerical methods and grid independency validation

The fluid–solid conjugated heat transfer problem is solved by the full-field computation method. The solid in the computational domain is regarded as a special fluid of infinite viscosity. The harmonic mean method is adopted for the interface diffusion coefficient. In order to guarantee the continuity of the flux rate at the interface, the thermal conductivity of the fin and fluid adopts individual values, while the heat capacity of the fin takes the value of the fluid. This is because in the nominal diffusion coefficient in the energy equation, Eq. (10), is k/c_p, and from the definition of the harmonic mean such practice is needed. For more details references [15,16] may be referred. The computational domain is discretized by nonuniform grids with the grids of the fin coil region being finer and those in the extension domains being coarser. The governing equations are discretized by the finite volume method [15], and the convection term is discretized by the power-law scheme. The coupling between pressure and velocity is implemented by the SIMPLE algorithm. The convergence criterion for the velocities is that the maximum relative mass residual of the cells is less than 1.0×10^{-6}, and the criterion for temperature is that the relative difference between the two heat transfer rates obtained from two iterations separated by 100 successive iterations is less than 1.0×10^{-6}.

In order to validate the solution independency of the grid, four different grid systems were investigated, they are: $78 \times 12 \times 12$, $142 \times 12 \times 12$, $142 \times 22 \times 12$, $142 \times 32 \times 12$. As shown in Fig. 4, at $Re = 1000$, the grid $142 \times 22 \times 12$ yields a Nu 1.0% higher than that of the finest grid $142 \times 32 \times 12$. So in this paper, in order to save the calculating time, the grid system $142 \times 22 \times 12$ was adopted for the computations of the average characters. However, in order to resolute the details of the local Nusselt number distributions around tube, the wavy crest and trough, a more finer grid system was adopted for those local characteristics. This practice will be described in the following presentation.

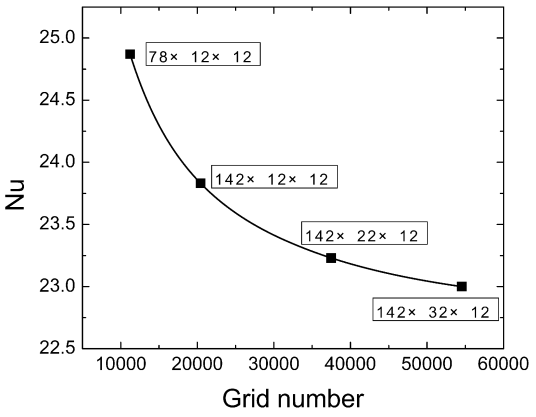

Fig. 4. Variation of the predicted Nusselt number with grid number systems at $Re = 1000$.

In our numerical simulation, the Reynolds number ranging from 500 to 4000 based on the tube outside diameter. A question may be raised that whether the laminar and steady model is appropriate. First, if we regard the flow between two adjacent fin surfaces as a channel flow, the transition Reynolds number may take the value of 2300, with the double spacing between the two fin surfaces as the reference dimension for the Reynolds number [17]. It should be noted that the tube outside diameter is usually 5–10 times of the fin spacing, so the values of the $Re = 2300$ (based on the fin spacing) correspond to the value around 6000–11 000 based on the tube diameter. Second, if we take the flow between two adjacent fin surfaces as the flow through a cylinder, the experimental data have shown that the turbulent flow occurs for $Re_d \geqslant 2 \times 10^5$ [17]. Third, recently, Xue and Min [18] performed a comparative study for flow in corrugated channels by using steady and transient models with the same conditions. They found that when the flow reaches periodic unsteady regime, it is appropriate to use steady model to predict the Nusselt number and friction factor. He et al. [19] conducted a comparison between steady and unsteady modes for plain plate fin-and-tube heat exchange at $Re = 5000$ based on tube outside diameter. It is found that the difference in the averaged Nusselt number between these two models is only about 0.35%. Many other numerical studies in the existing literature adopted the steady and laminar modes for heat exchanger surfaces, and reasonably good results are obtained. From the above discussion, for the studied case at the Reynolds number ranging from 500 to 4000, the laminar and steady model is still appropriate.

4. Simulation results and discussions

In this study, the body-fitted coordinate system was used to generate a general curvilinear coordinate system numerically by solving elliptic Poisson equations with proper control of grid densities. The 3D numerical simulation was performed on heat transfer characteristics of wavy fin-and-tube heat exchangers with fin efficiency effect accounted by the self-developed code. The major results are presented in the following section.

4.1. Parameter definitions

In order to present the simulation results, some parameters are defined as follows:

$$Re = U_c D/\upsilon, \qquad Nu = hD/k$$

$$h = Q/A\Delta T, \qquad Q = \dot{m} C_p(\overline{T}_{\mathrm{in}} - \overline{T}_{\mathrm{out}})$$

$$\overline{T} = \frac{\iint_A uT\,dA}{\iint_A u\,dA}, \qquad \Delta T = \frac{(T_{\mathrm{wt}} - \overline{T}_{\mathrm{in}}) - (T_{\mathrm{wt}} - \overline{T}_{\mathrm{out}})}{\ln[(T_{\mathrm{wt}} - \overline{T}_{\mathrm{in}})/(T_{\mathrm{wt}} - \overline{T}_{\mathrm{out}})]}$$

$$\overline{p} = \frac{\iint_A p\,dA}{\iint_A dA}, \qquad \Delta P = \overline{p}_{\mathrm{in}} - \overline{p}_{\mathrm{out}}$$

$$f = \Delta p D/\left[(1/2)\rho U_c^2 L\right] \tag{17}$$

where U_c, υ, k and C_p are the mean velocity in the minimum flow cross-section, viscosity, thermal conductivity and specific heat, D is the outside tube diameter, Δp is the pressure drop along the air flow direction, L is the fin length along the air flow direction, and A is the heat transfer surface which is determined by $A = A_o + A_f\eta$. The determination of the fin efficiency will be presented in the following discussion.

4.2. Comparisons of average heat transfer coefficient and friction factor

In order to validate the reliability of the numerical simulation procedure and the self-developed code, numerical simulations were carried out at the same operating conditions and fin geometrical configurations as presented in [20]. In Figs. 5 and 6, the comparisons of simulated average heat transfer coefficient and friction factor with the values calculated by experimental correlations[2,20] were performed under different Reynolds numbers ranging from 500 to 4000 (the corresponding frontal velocity ranges form 0.46 to 3.71 m s^{-1}).

As can be seen from the figures, the heat transfer coefficient increases and the friction factor decreases with the increase of Reynolds number. Compared to the Xin et al.'s experimental results [20], the mean deviation of *Nu* number is 3.3%, the max deviation is −6.0% for conditions other than Reynolds number at 500. When compared to the Wang et al.'s experimental results [2], the mean deviation of *Nu* number is 5.3%, the max deviation is 8.6%. The mean deviation of f between simulation results and experimental correlation [20] is 1.9%, the max deviation is 7.5%. It is worth noting that for numerical simulation of heat transfer and friction factor characteristics, such agreement between simulation and test correlation should be regarded rather good. Because in simulation, the model is perfect heat exchanger and many little details have been simplified. For example, the plain plate fin for the actual fin surface is not a perfect plain plate, there are some small bumpiness caused by manufacturing process. On the other hand, the experimental correlation itself has some deviation from their experimental data, usually being in the order of about 10–15%. Thus the good agreements between the predicted and tested results show the reliability of the physical model and the code developed.

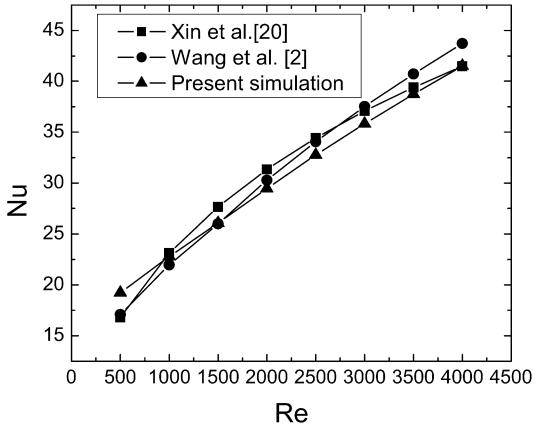

Fig. 5. Comparison of Nusselt number between prediction and test results.

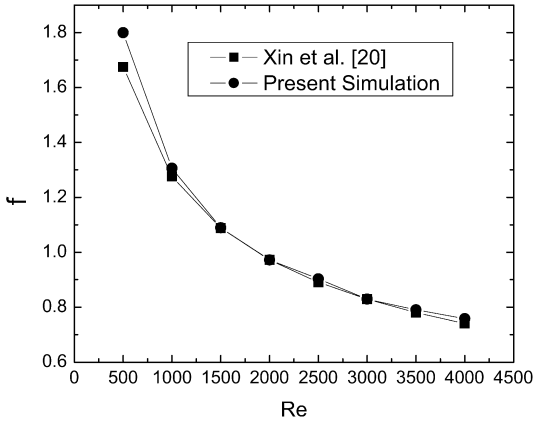

Fig. 6. Comparison of friction factor between prediction and test results.

4.3. Comparisons of average fin efficiency

Fig. 7 shows the comparison of predicted average fin efficiency to the values calculated by the Schmidt approximation [13] under different Reynolds numbers raging from 500 to 4000. The fin efficiency greatly depends on the fin thermal conductivity, in this paper fin thermal conductivity (k_f) is 236 W m^{-1} K^{-1}. The Schmidt approximation is expressed as follows.

$$\eta = \frac{\tanh(mr\phi)}{mr\phi} \tag{18}$$

where

$$m = \sqrt{\frac{2h_o}{k_f\delta_f}} \tag{19}$$

$$\phi = \left(\frac{R_{\text{eq}}}{r} - 1\right)\left[1 + 0.35\ln\left(\frac{R_{\text{eq}}}{r}\right)\right] \tag{20}$$

for staggered tube layout,

$$\frac{R_{\text{eq}}}{r} = 1.27\frac{X_M}{r}\left(\frac{X_L}{X_M} - 0.3\right)^{1/2} \tag{21a}$$

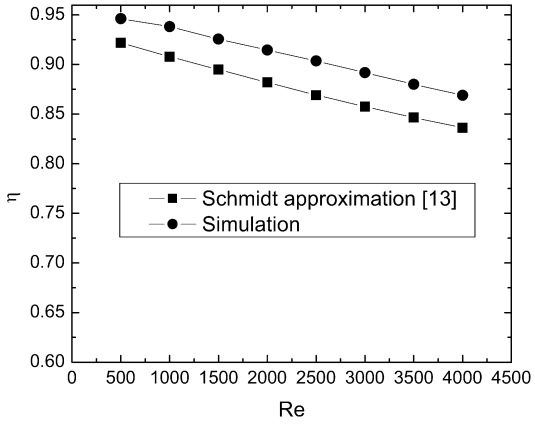

Fig. 7. Comparison of average fin efficiency between prediction and test results.

and for an inline layout, or 1-row coil,

$$\frac{R_{\mathrm{eq}}}{r} = 1.28\frac{X_M}{r}\left(\frac{X_L}{X_M} - 0.2\right)^{1/2} \tag{21b}$$

Because of the heat transfer coefficient predicted is a total value which includes fin surface effectiveness, as follows:

$$h_o = \frac{h}{\eta_o} \tag{22}$$

$$\eta_o = 1 - \frac{A_f}{A_o}(1-\eta) \tag{23}$$

So, the air-side heat transfer coefficient (h_o) and fin efficiency (η) need to be determined by iteration using Eqs. (18)–(23).

It can be seen form Fig. 7 that although the predicted η is larger than that calculated by Schmidt approximation, the difference between them is quite small. The mean deviation of η between numerical prediction and Schmidt calculation is 3.6%, and the max deviation is 4.0%. It can also be seen that with the increase of the Reynolds number, the fin efficiency decreases and in the computational conditions when Reynolds number is changing from 500 to 4000, fin efficiency decreases from 94.6% to 86.9%. The good agreement between the predicted results and Schmidt approximation shows the reliability of the developed code to predict the wavy fin efficiency. On the other hand, our numerical simulation of the fin efficiency is based on the strict definition of heat transfer theory, while Schmidt's method is an approximation. The good agreement of the two results shows that Schmidt's approximation is suitable for engineering design.

4.4. Distributions of local Nusselt number, local fin efficiency and temperature

A lot of papers had studied the average heat transfer and flow characteristics of wavy fin-and-tube heat exchangers numerically or experimentally. But because it is difficult to measure the temperature distributions on the whole fin surface and flow domain, the local heat transfer coefficient and local fin efficiency are not easy to be obtained experimentally.

For a regular rectangle channel with either constant wall temperature or constant wall heat flux, when flow gets fully developed, the local Nusselt number is constant. But to the wavy fin-and-tube heat exchangers, there are wavy angle, tube, and fin efficiency, all of which would affect the local temperature distribution and heat flux, so the distribution of the local Nusselt number and local fin efficiency are complicated and irregular. In the present study, in order to simulate the distributions of the local Nusselt number and fin efficiency accurately, the grid distributions around the tube surface, wave crest and wave trough are made more denser than that adopted in the grid-independency examination, which is shown in Fig. 8.

The local Nusselt number and fin efficiency are obtained by the following equations

$$Nu_{i,j} = \frac{\dot{q}_{w,i,j} D}{k(T_{w,i,j} - T_{b,i,j})} \tag{24}$$

$$\eta_{i,j} = \frac{T_{w,i,j} - T_{b,i,j}}{T_{\mathrm{wt}} - T_{b,i,j}} \tag{25}$$

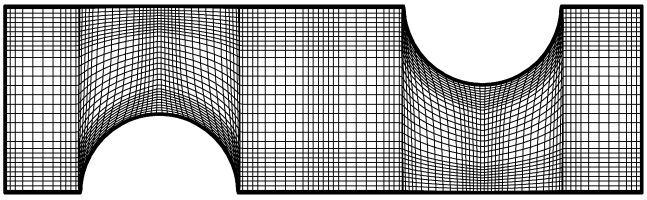

Fig. 8. Grid system being made denser around the tube surface, wave crest and wave trough.

where $\dot{q}_{w,i,j}$, $T_{w,i,j}$, and T_{wt} are the local heat flux, local temperature on fin surface and temperature on tube surface; the fluid bulk temperature $T_{b,i,j}$ is defined as

$$T_{b,i,j} = \int TU\,dA \Big/ \int U\,dA \tag{26}$$

The local average Nusselt number and fin efficiency in y-direction are defined as:

$$Nu_i = \frac{\sum_j Nu_{i,j} A_{i,j}}{\sum_j A_{i,j}} \tag{27}$$

$$\eta_i = \frac{\sum_j \eta_{i,j} A_{i,j}}{\sum_j A_{i,j}} \tag{28}$$

As the baseline, Fig. 9 shows the distributions of the local Nusselt number, fin efficiency and temperature at $F_p = 1.2$ mm for the plain plate fin (wavy angle $\alpha = 0°$). Figs. 9(a) and (b) shows that the local Nusselt number is very large at inlet region and then decreases along the flow direction. At the outlet region, the local Nusselt number is very much smaller compared with that at the inlet region. These conclusions are coincident with the results of Chen et al. [21]. In order to investigate the local heat transfer coefficient on the fin of one-tube plain plate finned-tube heat exchangers, they divided the whole plate fin surface into 6 sub-fin regions, and the heat transfer coefficient on each sub-fin region is assumed to be a constant value. They analyzed the 6 average local heat transfer coefficients on the sub-fin surfaces and found the ratio of the average heat transfer coefficient in the front region to that in the back region can be up to 10. In the present study, it can also be seen that at the front of the tube region because of the cross section decreases and the velocity increases, the decreasing tend of the local Nusselt number is slower. And at the tube back region the local Nusselt number is quickly decreased due to the decreasing of velocity and flow separation, which indicates that at this region, the convective heat transfer is weak, and we can improve the total heat transfer coefficient by enhancing the local Nusselt number of this region. The local fin efficiency as a whole increases along the fluid flow direction, as shown in Fig. 9(c) and (d). At the inlet region, due to the high local heat transfer coefficient and low local temperature, the value is very small, and then it increases quickly. At the tube region the increasing tend is slower because of the high local temperature. At the back region of tube, the local fin efficiency has a decrease due to the decreasing of the local temperature, and then it repeats the foregoing variation process. For comparison purposes, the temperature distributions at the whole plain plate fin surface (x–y plane) and along the flow direction at middle section (x–z

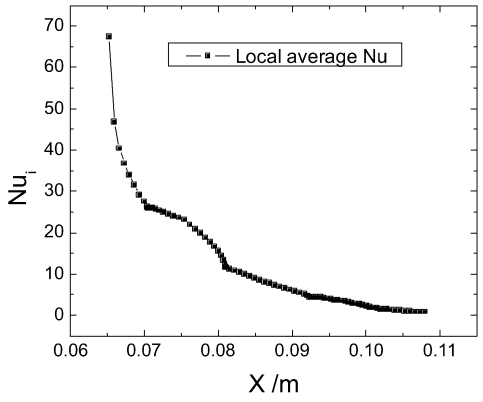

(a) Local average Nu number of y-direction Nu_i variation along x-direction

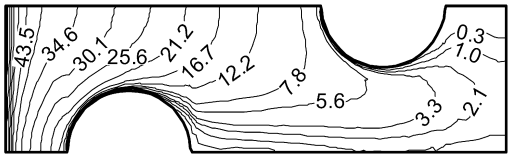

(b) Local Nusselt number distribution on the whole fin surface

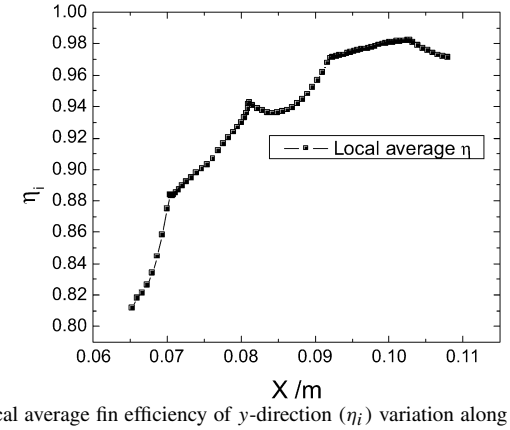

(c) Local average fin efficiency of y-direction (η_i) variation along the flow direction

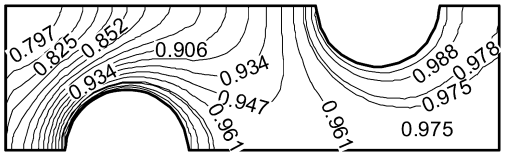

(d) Local fin efficiency distribution on the whole fin surface

Fig. 9. Distributions of local Nusselt number, fin efficiency and temperature in $\alpha = 0°$, $Re = 1000$.

plane) are shown in Fig. 9(e) and (f). In Fig. 9(f) the temperature distributions are separated into two parts along the x-direction with the same length, on the scale of 1, and at z-direction on the scale of 2.

By the analysis of the local Nusselt number distributions, such conclusions can be gained that in fin-and-tube heat exchangers the heat transfer coefficient at inlet region is much larger than that at the outlet region, so the convective heat transfer mostly occurs at the inlet region.

Figs. 10 and 11 show the distributions of the local Nusselt number, fin efficiency and temperature at $F_p = 1.2$ mm for wavy angle $\alpha = 10°$, $20°$ respectively. As shown in Fig. 10, because of the small wavy angle $\alpha = 10°$, the effects of wavy

(e)Temperature distribution on the fin surface

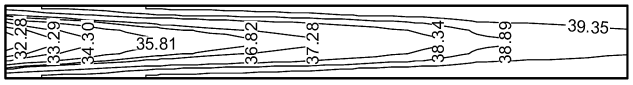

Temperature distribution on the middle section-1

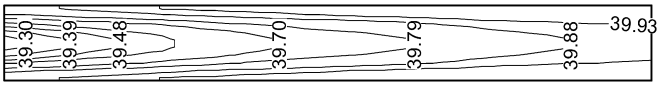

Temperature distribution on the middle section-2

(f) Temperature distribution on the middle section of x–z plane

Fig. 9. (*continued*)

angle on the distributions of the local Nusselt number, fin efficiency and temperature are not obvious, the distributions are similar to those of plain plate fin. But the existence of wavy angle causes the local Nusselt number and fin efficiency distributions are not as regular as the plain plate fin and present some fluctuation. The effect of wavy angle on the distributions of the local Nusselt number, fin efficiency and temperature can be seen clearly in Fig. 11 for wavy angle $\alpha = 20°$.

Fig. 11(a) and (b) shows the computed local Nusselt number distributions for $\alpha = 20°$. Generally speaking, the local Nusselt number decreases along the flow direction which is similar to plain plate fin, but the detailed variation is more complicated. The local Nusselt number decreases sharply at the inlet region, and then it increases near to the first wave crest due to the wave crest breaking the heat transfer boundary layer. After the first wave crest, it decreases sharply again because here the flow separation occurs, and then it decreases slowly up to the first wave trough where the local Nusselt number becomes a relative minimum due to a reversed corner flow. At every wave crest and wave trough we find the similar trend, the only difference is the degree of variation. The local fin efficiency as a whole increases along the fluid flow direction and at the back region of the tube, the local fin efficiency has a decrease, as shown in Fig. 11(c) and (d), which is the same as that of the plain plate fin. But at inlet region and the wave crest or wave trough, due to the effect of local Nusselt number and temperature, the fin efficiency distribution present obvious fluctuation. The temperature distributions of fin surface and middle section in x–z plane are expressed in Fig. 10(e), (f) and Fig. 11(e), (f) for wavy angle of 10 and 20°, respectively. And in Fig. 10(f) and Fig. 11(f), the schematic diagrams were presented on the scale of 1 in x-direction and 2 in z-direction.

From Figs. 9–11, we can see the distributions of local Nusselt number, fin efficiency and temperature on fin surface of wavy fin-and-tube heat exchanger are more complicated and irregular than those of plain plate fin. The wavy angle can greatly affect the distributions of local variables, the larger of the wavy angle value, the more distinct of the effects.

Based on the prediction results, it is clear that the fin efficiency and heat transfer coefficient varies locally. For example,

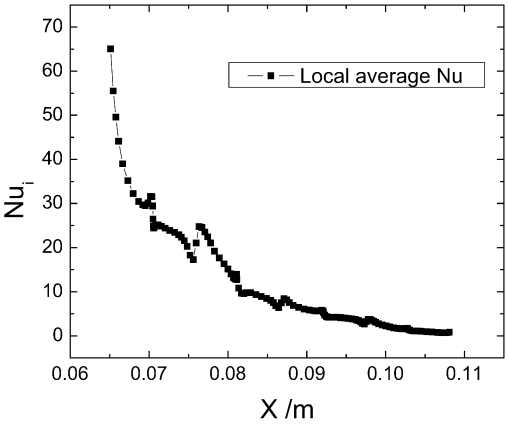

(a) Nu_i variation along x-direction

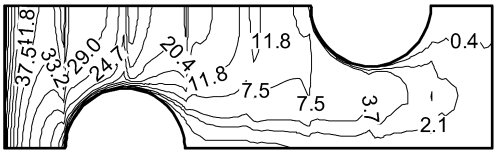

(b) Local Nusselt number distribution on the whole fin surface

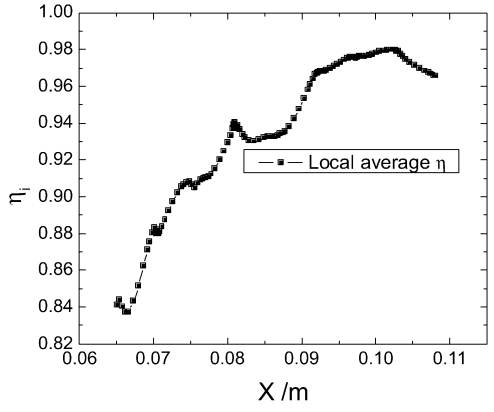

(c) η_i variation along x-direction

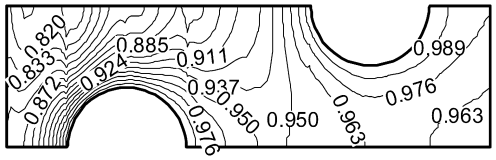

(d) Fin efficiency distribution on the whole fin surface

Fig. 10. Distributions of local Nusselt number, fin efficiency and temperature in $\alpha = 10°$, $Re = 1000$.

the fin efficiency at the inlet region of wavy fin is larger than that of plain plate fin, by replacing the plain fin with wavy fin cannot only increase average Nusselt number but also improve the local fin efficiency at the inlet. For fin-and-tube heat exchangers the heat transfer coefficient at inlet region is much larger than that at the outlet region and the convective heat transfer mostly occurs at the inlet region. Thus by increase the fin area and wavy angle at the inlet and decrease the fin area and wavy angle at the outlet could not only enhance heat transfer but also decrease material consumes and pressure drop.

In Fig. 12, the distributions of local Nusselt number and fin efficiency are presented at different *Re* numbers for $F_p = 1.2$ mm, wavy angle $\alpha = 10^0$. It can be seen that the variation

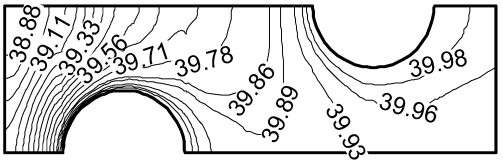

(e)Temperature distribution on the fin surface

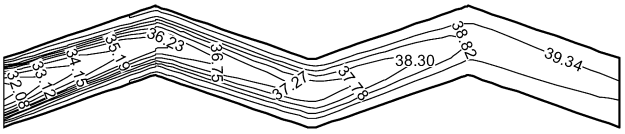

Temperature distribution on the middle section-1

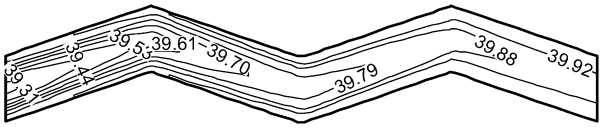

Temperature distribution on the middle section-2

(f) Temperature distribution on the middle section of x–z plane

Fig. 10. (*continued*)

trends along the x-direction at different *Re* numbers are very similar. The effects of the wave crest and wave trough on the distributions of the local Nusselt number and fin efficiency increase with the increasing of *Re* number.

5. Conclusions

In this paper, the BFC method was adopted to generate 3D computational grids, then the air side heat transfer and fluid flow characteristics of wavy fin-and-tube heat exchanger were performed by taking into account the fin efficiency effect. The simulation results of average Nusselt number, friction factor and fin efficiency were compared with experimental correlations and Schmidt approximations, the good agreements validate the model code. The local Nusselt number, fin efficiency and temperature distributions on fin surface at different wavy angle ranging from 0° (plain plate fin) to 20° were studied. The following conclusions can be made:

(1) The average Nusselt number of the wavy fin-and-tube heat exchanger increases with the increase of Reynolds number, but the friction factor and average fin efficiency decrease.
(2) For the plain plate fin, the local Nusselt number decreases quickly along the flow direction, at the outlet region, it is much smaller compared with the values of the inlet region, and at the back region of tube, the local Nusselt number has a drastic decrease, which are coincident with the results of Ref. [21]. Because the local Nusselt number at the inlet is much larger than that at the outlet, and the convective heat transfer mostly occurs at the inlet region, an appropriate increase of the fin area at the inlet and decrease of the fin area at the outlet cannot only enhancing heat transfer but also decreasing material consume. The local fin efficiency increases along the flow direction due to the effect of local Nusselt number and temperature: at the inlet the fin efficiency is very low, it increases along the flow direction and then after the tube the fin efficiency decreases.

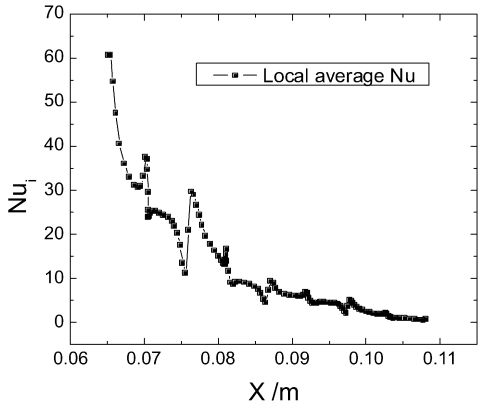

(a) Nu_i variation along x-direction

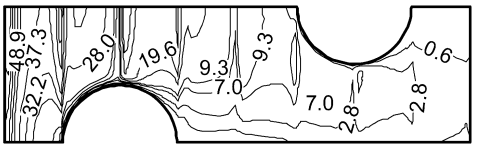

(b) Local *Nu* number distribution on the whole fin surface

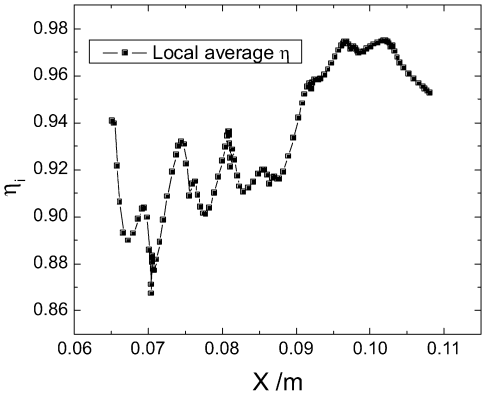

(c) η_i variation along x-direction

(d) Fin efficiency distribution on the whole fin surface

Fig. 11. Distributions of local Nusselt number, fin efficiency and temperature in $\alpha = 20°$, $Re = 1000$.

(3) For wavy fins, the distributions of the local Nusselt number, local fin efficiency are more complicated due to the effect of the wavy angle. The local Nusselt number decreases sharply at the inlet region, and then it increases at near to the first wave crest. After the first wave crest, it decreases sharply again, and then it decreases slowly up to the first wave trough where the local Nusselt number becomes a relative minimum. At every wave crests and wave troughs, the trend is similar, only difference is in variation degree. The larger value of the wavy angle, the more distinctness of the phenomenon. At inlet region and the wave crest or wave trough, due to the effect of local Nusselt number and temperature, the fin efficiency distribution presents obvious irregular fluctuation.

(e) Fin temperature distribution on the fin surface

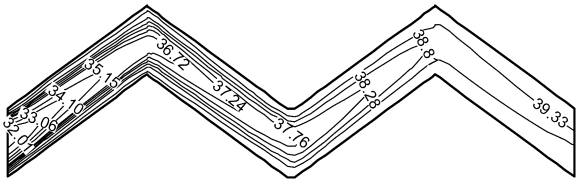

Temperature distribution on the middle section-1

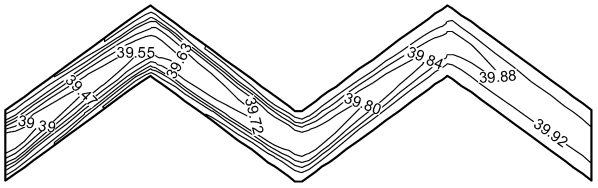

Temperature distribution on the middle section-2

(f) Temperature distribution on the middle section of x–z plane

Fig. 11. (*continued*)

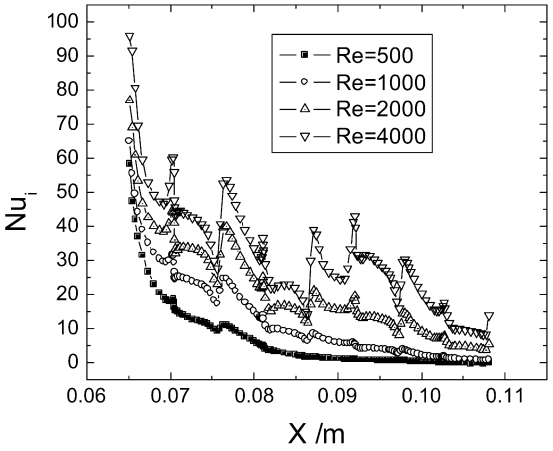

(a) Nu_i variations along x-direction at different *Re* numbers

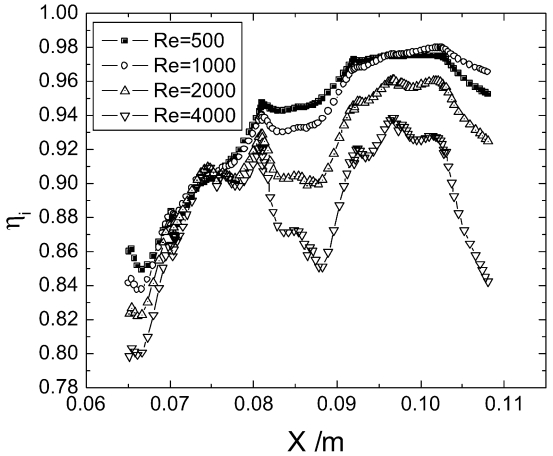

(b) η_i variations along x-direction at different *Re* numbers

Fig. 12. Distributions of local Nusselt number and fin efficiency at different *Re* numbers in $\alpha = 10°$.

(4) The fin efficiency at the inlet region of wavy fin is larger than that of plain plate fin. And for fin-and-tube heat exchangers the heat transfer coefficient at inlet region is very larger than that at the outlet region and the convective heat transfer mostly occurs at the inlet region. We can appropriately increase the fin area and wavy angle at the inlet and decrease the fin area and wavy angle at the outlet, which could not only enhance heat transfer but also decrease material consume and pressure drop.

References

[1] C.C. Wang, W.L. Fu, C.T. Chang, Heat transfer and friction characteristics of typical wavy fin-and-tube heat exchangers, Heat Transfer Friction Characteristics 14 (1997) 174–186.

[2] C.C. Wang, Y.M. Hwang, Y.T. Lin, Empirical correlations for heat transfer and flow friction characteristics of herringbone wavy fin-and-tube heat exchangers, Int. J. Refrig. 25 (2002) 673–680.

[3] S. Wongwises, Y. Chokeman, Effect of fin pitch and number of tube rows on the air side performance of herringbone wavy fin and tube heat exchangers, Energy Convers. Management 46 (2005) 2216–2231.

[4] J.Y. Jang, L.K. Chen, Numerical analysis of heat transfer and fluid flow in a three-dimensional wavy-fin and tube heat exchanger, Int. J. Heat Mass Transfer 40 (16) (1997) 3981–3990.

[5] R.M. Manglik, J.H. Zhang, A. Muley, Low Reynolds number forced convection in three-dimensional wavy-plate-fin compact channels: fin density effects, Int. J. Heat Mass Transfer 48 (2005) 1439–1449.

[6] H. Zabronsky, Temperature distribution and efficiency of a heat exchanger using square fins on round tubes, ASME J. Appl. Mech. 22 (1955) 119–122.

[7] D.Y. Kuan, R. Aris, H. T Davis, Estimation of fin efficiencies of regular tubes arrayed in circumferential fins, Int. J. Heat Mass Transfer 27 (1984) 148–151.

[8] H.T. Chen, J.T. Liou, Optimum dimensions of the continuous plate fin for various tube arrays, Numer. Heat Transfer, Part A 34 (1998) 151–167.

[9] T.V. Jones and C.M.B. Russell, Efficiency of rectangular fins, in: ASME/AIChE National Heat Transfer Conference, Orlando, Florida, 1980, pp. 27–30.

[10] F.E.M. Saboya, E.M. Sparrow, Local and average heat transfer coefficients for one-row plate fin and tube heat exchanger configurations, ASME J. Heat Transfer 96 (1974) 265–272.

[11] E.C. Rosman, P. Carajilescov, F.E.M. Saboya, Performance of one- and two-row tube and plate fin heat exchangers, ASME J. Heat Transfer (1984) 627–632.

[12] H. Ay, J.Y. Jang, J.N. Yeh, Local heat transfer measurements of plate finned-tube heat exchangers by infrared thermography, Int. J. Heat Mass Transfer 45 (2002) 4069–4087.

[13] T.E. Schmidt, Heat transfer calculations for extended surfaces, Refrigerating Engineering (April 1949) 351–357.

[14] J.F. Thompson, F.C. Thames, C.W. Mastin, Automatic numerical generation of body-fitted curvilinear coordinate system for field containing any number of arbitrary two-dimensional bodies, J. Compt. Phys. 15 (1974) 299–319.

[15] W.Q. Tao, Numerical Heat Transfer, second ed., Xi'an Jiaotong University Press, Xi'an, 2001.

[16] Z.G. Qu, W.Q. Tao, Y.L. He, Three-dimensional numerical simulation on laminar heat transfer and fluid flow characteristics of strip fin surfaces with X-arrangement of strips, ASME J. Heat Transfer 126 (4) (2004) 697–707.

[17] F.P. Incropera, D.P. DeWitt, Fundamentals of Heat, fifth ed., John Wiley & Sons, New York, 2002, pp. 408–495.

[18] W. Xue, J.C. Min, Numerical predictions of fluid flow and heat transfer in corrugated channels, in: Proceedings of the 3rd International Symposium on Heat Transfer and Energy Conservation, 1, Guangzhou, China, January 12–15, 2004, pp. 714–721.

[19] Y.L. He, W.Q. Tao, F.Q. Song, W. Zhang, Three-dimensional numerical study of heat transfer characteristics of plain plate fin-and-tube heat exchangers from view point of field synergy principle, Int. J. Heat Fluid Flow 26 (2005) 459–473.

[20] R.C. Xin, H.Z. Li, H.J. Kang, W. Li, W.Q. Tao, An experimental investigation on heat transfer and pressure drop characteristics of triangular wavy fin-and-tube heat exchanger surfaces, J. Xi'an Jiaotong Univ. 28 (2) (1994) 77–83.

[21] H.T. Chen, J.P. Song, Y.T. Wang, Prediction of heat transfer coefficient on the fin inside one-tube plate finned-tube heat exchangers, Int. J. Heat Mass Transfer 48 (2005) 2697–2707.